Journal of Physics:
Conference Series

PAPER • **OPEN ACCESS**

Experimental investigation of the burning rate of solid propellant rocket motors

To cite this article: M. Abdelmaksoud *et al* 2025 *J. Phys.: Conf. Ser.* **3070** 012018

Experimental investigation of the burning rate of solid propellant rocket motors

M. Abdelmaksoud[1*], A.M. Abdelall[2], M.A. Al-Sanabawy[1] and A. Hashish[1]

[1] Aerospace Engineering Department, Military Technical College, Cairo, Egypt
[2] Chemical Engineering Department, Military Technical College, Cairo, Egypt

[*]E-mail: abdelmaksoud911912@gmail.com

Abstract. The burning rate of solid propellant is a critical parameter influencing the performance and stability of rocket motors. This study experimentally investigates the burning rate of composite solid propellant used in dual-thrust rocket motors through both static firing tests and acoustic emission strand burner tests. A standard sub-scale 2-inch motor is employed to measure dynamic burning rate under varying combustion chamber pressure, while strand burner tests provide static burning rate measurements. The experimental results reveal a deviation between static and dynamic burning rates, attributed to erosive burning effects. Additionally, an internal ballistics prediction module (IBPM) is validated by comparing its outputs with static firing test data, demonstrating its applicability for performance prediction. The findings provide essential insights into the influence of combustion conditions on burning rate characteristics, targeting improved modelling and optimization of dual-thrust solid rocket motors (DTRMs).

Keywords: Burning rate, Static test, Strand burner and IBPM.

1. Introduction

The burning rate is a fundamental parameter that governs the ballistic performance of solid rocket propellants and serves as a key factor in evaluating the overall efficiency of rocket motor design[1]. Since the burning rate follows an exponential relationship, precise control throughout the combustion process is essential to prevent excessive chamber pressure buildup, as well as to mitigate abnormal combustion behaviors such as unstable or interrupted burning, chuffing[2], and pressure oscillations. Several factors influence the burning rate, including combustion chamber pressure, initial propellant temperature, composition formulation[3, 4], grain geometry, erosive burning effects, and motor vibrations.

Achieving a smooth and accurate transition from small-scale strand burner tests to sub-scale motors and ultimately to full-scale motor is a major challenge in the solid rocket propellant industry. High-precision burning rate measurements across these scaling stages are crucial for ensuring reliable performance and safety in rocket propulsion systems[5]. Some solid propellant burning rate measuring techniques are performed via strand burner with impeded wires[6], ultrasonic pulse-echo technique[7], microwave technique[8] and acoustic emission technique[9]. Measuring burning rate and formulation of a convenient burning law mark an essential step to facilitate dual-thrust solid propellant rocket motors design.

DTRMs play a critical role in contemporary missile and rocket propulsion systems, providing a propulsion mechanism that enables both high acceleration and sustained flight. Unlike conventional solid propellant motors, which generate a smooth thrust profile, DTRMs are engineered to deliver two distinct thrust phases: an initial high-thrust boost phase followed by a lower-thrust sustain phase. This biphasic thrust operation is essential for military and aerospace applications, including anti-aircraft and anti-armor missile systems, where rapid acceleration is required to engage a target, followed by controlled propulsion to maintain the designated trajectory[10].

The design of a DTRM necessitates meticulous selection of propellant formulations, grain geometry, and motor configuration. The simplest DTRM configuration consists of a single chamber with a nozzle; however, advanced architectures may incorporate multiple combustion chambers, intermediate nozzles, or variable-geometry nozzles to enhance thrust control. Such design flexibility allows for the customization of DTRMs according to specific mission profiles, optimizing their efficacy for tactical applications that require precision and efficiency[11].

DTRMs exhibit several advantages over alternative propulsion technologies, including enhanced reliability, ease of storage and handling, and an extended operational lifespan due to their relatively simple structural configuration and minimal reliance on moving components. Their ability to generate a tailored thrust-time profile renders them particularly advantageous for missions necessitating rapid acceleration followed by regulated cruising velocity. Advances in propellant chemistry, grain design, and motor engineering continue to drive the evolution of DTRM technology, expanding its applicability to next-generation missile systems and other aerospace applications[12].

During the initial phase of solid propellant rocket motor design, it is essential to identify and quantitatively assess deviations of internal ballistic parameters from ideal conditions. In early-stage development, there are differences between theoretical performance predictions and actual test results of standard ballistic motors. Modern numerical methods serve as effective tools for analyzing combustion dynamics and gas flow in solid propellant rocket motors with specific designs. Numerical simulations facilitate the investigation of key physical processes, contributing to performance optimization and cost reduction in the development of advanced rocket systems[13].

This study aims to investigate the burning rate of solid propellant rocket motors through scheduled static firing tests and acoustic emission strand burner tests in order to clarify the difference between static and dynamic burning rate. In addition, an IBPM is validated by static firing test of a standard sub-scale 2-inch motor.

2. Case study

A standard sub-scale 2-inch motor is shown in Figure 1 while a 3D model of the composite propellant grain is shown in Figure 2. The dimensions of the composite propellant grain were selected from previous work to maintain constant burning area and accordingly constant combustion chamber pressure. The test motor is used to predict burning rate law and to validate burn-back analysis module and IBPM. This marks an essential step for DTRM design.

Composite solid propellant used in this study has 86% solid components (69% ammonium perchlorate as oxidizer and 17% aluminium powder as fuel) and 14% binder.

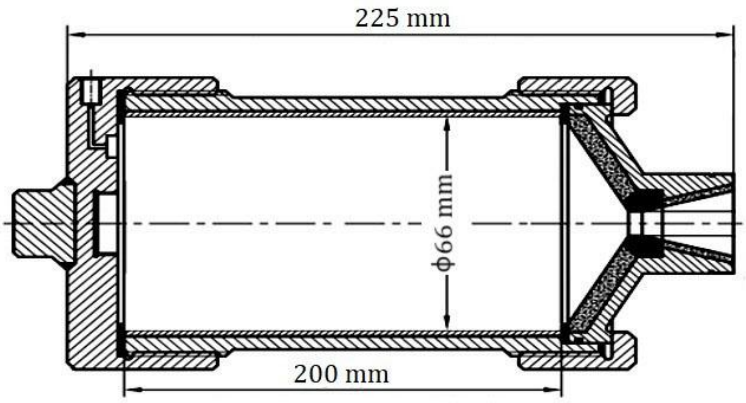

Figure 1. Standard sub-scale 2-inch motor.

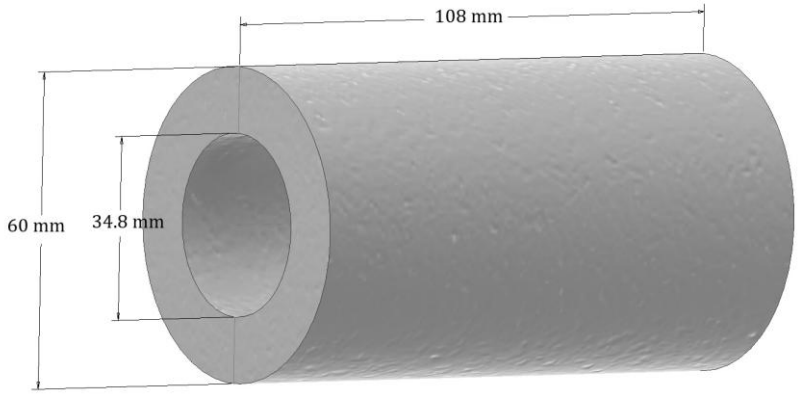

Figure 2. Standard sub-scale 2-inch motor grain.

3. Methodology

A detailed discussion of the composite propellant manufacturing will be provided. Then, the two techniques for the burning rate measurement will be discussed. Finally, the burn-back analysis and the IBPM will be explained.

3.1 composite propellant manufacturing

The propellant is prepared using vertical mixer and casted in six 2-inch motor moulds and a propellant block mould, Figure 3. The moulds are left in oven for 6 days at 50 ℃ to be cured. After curing process, the 2-inch motors are demolded and cleared from excess propellant. The sub-scale motors are checked by x-ray to ensure absence of cracks or air bubbles in the grain, Figure 4. Also, the propellant block is checked to avoid any cracks or air bubbles.

The propellant mould is cut using pneumatic cutter, Figure 5, into samples with specific dimentions (6mm width, 6mm thickness and 120mm length). The sub-scale motors are used to determine dynamic burning rate through static firing test while strips samples are used to determine static burning rate through acoustic emission strand burner test.

Figure 3. Propellant block mould and 2-inch motor moulds.

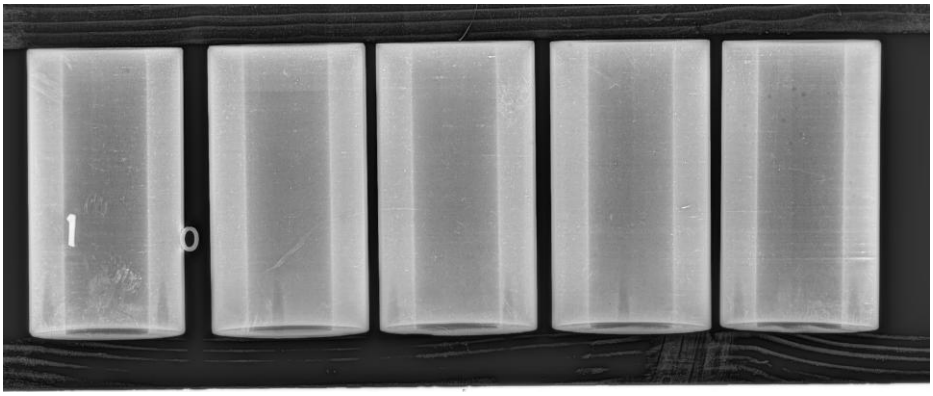

Figure 4. X-ray examination of grains.

Figure 5. Strip samples pneumatic cutter.

3.2 Measurement of the burning rate

Two test facilities are used to measuring the burning rate comprising static firing test and acoustic emission strand burner test.

3.2.1 Static firing test

The sub-scale 2-inch motors are prepared with various throat diameters (6, 7 and 8 mm) to achieve different operating pressures and hence different burning rates. Then, the test motors are stored in normal condition at 20 °C for certain time before testing and then assembled on the test stand. A pressure transducer, connected to the data acquisition system, is mounted to the test motor before the firing, Figure 6. A block diagram for the static firing test facility is illustrated in Figure 7.

Figure 6. Static firing test assembly.

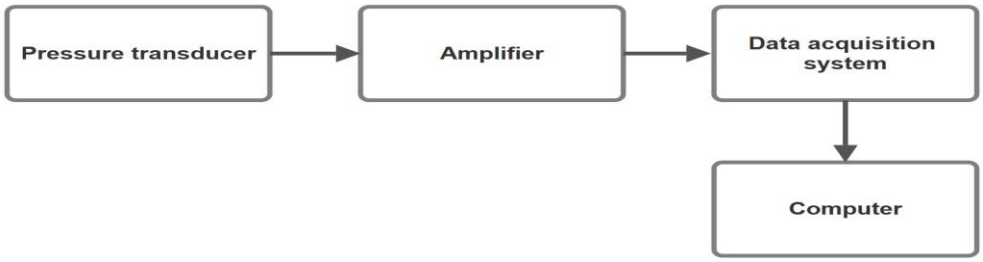

Figure 7. Static firing test block diagram.

3.2.2 Acoustic emission strand burner test

The solid propellant samples are placed in a water-filled combustion chamber and secured in the sample holder using Ni-Cr wire as presented in Figure 8. The chamber is pressurized with Nitrogen at varying levels between 5 and 10 MPa, while the operating temperature is maintained at 20°C.

Figure 8. Specimen fixation.

Ignition is initiated electrically using an 18 V, 2 A current. Following ignition, combustion propagates in a downward direction, generating acoustic waves throughout the burning process. The acoustic emission signals produced during combustion are transmitted through the chamber and detected by an acoustic transducer, and converted into electrical signals. These signals are amplified and transmitted to data acquisition system for processing and analysis, Figure 9.

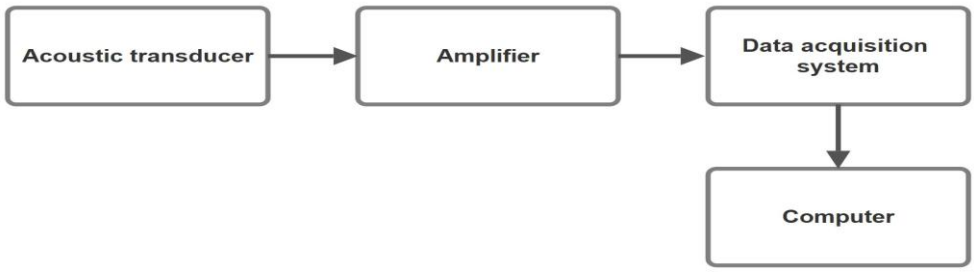

Figure 9. Acoustic emission strand burner test block diagram.

The time counter is stopped upon the completion of combustion and burning rate at each specified pressure is determined using the equation:

$$r = \frac{L}{\Delta t} \quad (1)$$

where, r (mm/s) is burning rate, L (mm) is the specimen length and t (s) is time between start and end of combustion.

3.3 Burn-back analysis and IBPM

Grain regression is modelled by applying a uniform web increment in all directions. A specific web increment is chosen for which the regression is calculated. At each step, the grain geometry is automatically updated to reflect the new regression state[14].

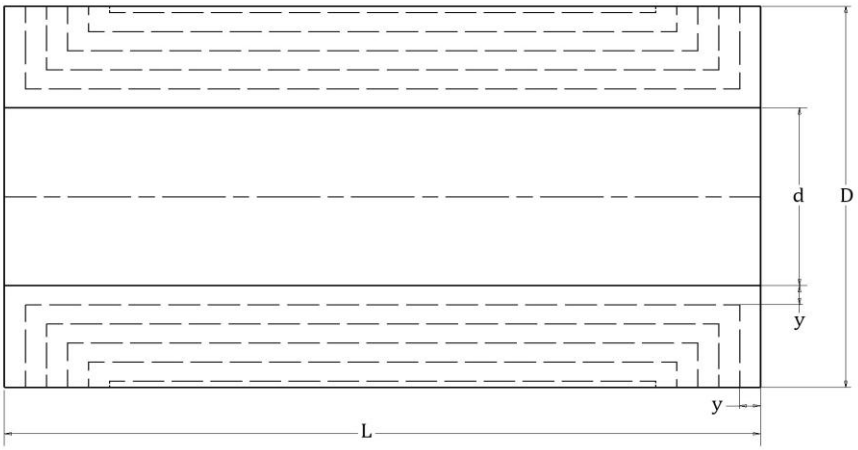

Figure 10. Regression at sub-scale motor's grain.

A MATLAB module is coded to generate the burning surface area at each step (Figure 10) based on following equation:

$$A = \left(\frac{\pi}{2}(D^2 - (d + 2y)^2)\right) + \left(\pi(d + 2y)(L - 2y)\right) \quad (2)$$

where, A is the surface burning area, D is the outer diameter of the grain (60 mm), d is the inner diameter of the grain (34.8 mm), L is the length of the grain (108 mm) and y is the step of regression.

The output data of the surface burning area updated at each step and updated inputs are used by IBPM and generates P-T curve according to the following equation[15]:

$$V_c \frac{dP_c}{dt} = \rho_{sp} R T_C A_b a P_c^{\,n} - \Gamma P_c A_{cr} \sqrt{R T_c} \quad (3)$$

$$\Gamma = \sqrt{\gamma}\left(\frac{2}{\gamma+1}\right)^{\frac{\gamma+1}{2(\gamma-1)}} \quad (4)$$

where, V_c is free volume of combustion chamber, P_c is pressure of combustion, ρ is propellant density, T_c is combustion temperature, A_b is burning area, a is burning law constant, n is pressure exponent, γ is specific heat ratio, A_{cr} is the critical area and R is gas constant. A flowchart for the IBPM is illustrated in Figure 11.

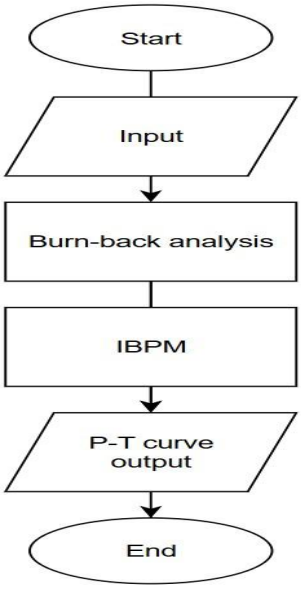

Figure 11. Flowchart of P-T curve generation process.

4. Results & Discussion

Table 1 represents burning rates measured experimentally from both static firing test and strand burner test. The static test was done with different nozzles throat diameters (6, 7 and 8 mm respectively) to obtain different burning rates. Each throat diameter was used by two motors to confirm measured data. Strand burner test was done at different pressures to maintain different burning rates.

Output data had been analysed by using ln-ln scale represented in Figure 12 where a (burning law constant) and n (pressure exponent) were maintained from linear trendline equation, Table2. The burning rate had been calculated using the following equation:

$$r = ap^n \quad (5)$$

From static firing and strand burner test results, burning rate had been calculated at 6.895MPa (1000 psi) which equals 6.4 mm/s and 6.1 mm/s respectively with deviation 4.7%, the higher burning rate of 2-inch motor may be attributed to erosive burning[16] and measurement uncertainties.

The IBPM is verified by comparing it with experimental data from static firing test as illustrated in Figure 13.

Table 1. Data from static firing test and acoustic emission strand burner test.

	Static firing test		Strand burner test	
	P (MPa)	r (mm/s)	P (MPa)	r (mm/s)
1	11.548	7.57	10.239	6.952
2	11.332	7.55	9.015	6.563
3	7.104	6.52	8.024	6.315
4	7.017	6.41	6.986	6.006
5	5.124	6.07	6.14	5.825
6	5.091	6.06	5.141	5.52

Table 2. Comparison between a and n values.

Static firing test		Strand burner test	
a	n	a	n
3.76	0.28	3.28	0.32

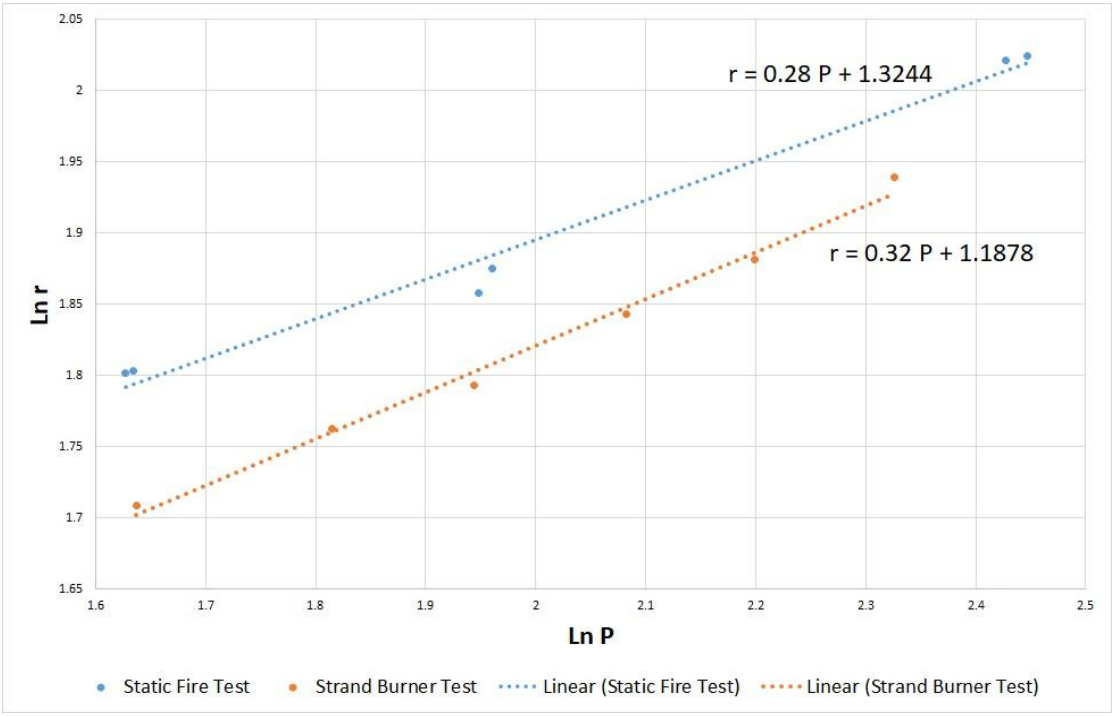

Figure 12. Static firing test and acoustic emission strand burner test ballistic nomogram.

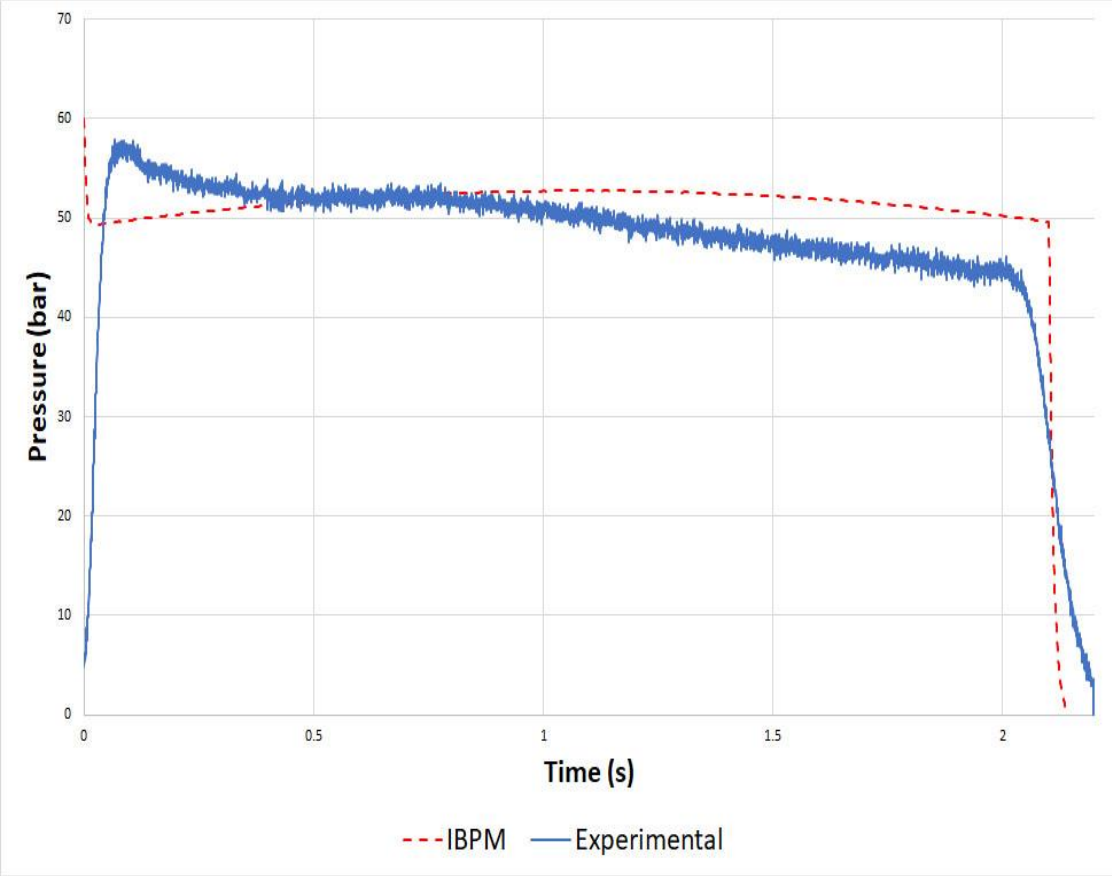

Figure 13. IBPM compared to experimental.

5. Conclusion

The strand burner test offers several advantages over static firing tests. It eliminates the need for inhibitors or complex wiring and requires only a small specimen, reducing experimental costs. Additionally, samples can be extracted from large-scale motors for testing. The acoustic emission strand burner technique presents a viable method for accurately estimating the burning rate of aged propellant in large-scale motors, provided the associated measurement uncertainties are considered.

The variation between the burning rates obtained from strand burner tests (static conditions) and static firing tests (dynamic conditions) arises due to erosive burning effects. Moreover, even a slight variation in the pressure exponent can result in significant changes in chamber pressure, a critical factor that must be accounted for in motor design. The IBPM is verified on sub-scale tubular 2-inch motors and can be developed to be used for DTRMs.

References

[1] A. Aziz, R. Mamat, and W. W. Ali, "Development of strand burner for solid propellant burning rate studies," in *IOP Conference Series: Materials Science and Engineering*, 2013, vol. 50, no. 1: IOP Publishing, p. 012048.
[2] T. A. Angelus and R. A. Yount, "Chuffing and nonacoustic instability phenomena in solid propellant rockets," *AIAA Journal,* vol. 2, pp. 1307-1313, 1964.
[3] G. Gore, K. Tipare, R. Bhatewara, U. Prasad, M. Gupta, and S. Mane, "Evaluation of ferrocene derivatives as burn rate modifiers in AP/HTPB-based composite propellants," *Defence Science Journal,* vol. 49, no. 2, p. 151, 1999.
[4] M. Kohga and S. Togo, "Influence of iron oxide on thermal decomposition behavior and burning characteristics of ammonium nitrate/ammonium perchlorate-based composite propellants," *Combustion and Flame,* vol. 192, pp. 10-24, 2018.
[5] E. Elsaka, S. Elbasuney, H. E. Mostafa, T. Elhedery, and A. Eldakhakhny, "Burning rate measurement of composite propellant using acoustic wave emission in comparison with other techniques," *Journal of Engineering Science and Military Technologies,* vol. 4, no. 2, pp. 226-232, 2020.
[6] B. Crawford, C. Huggett, F. Daniels, and R. Wilfong, "Direct determination of burning rates of propellant powders," *Analytical Chemistry,* vol. 19, no. 9, pp. 630-633, 1947.
[7] D. Deepak, R. Jeenu, and P. Sridharan, "Application of Ultrasonic Technique for Measurement of Instantaneous Burn Rate of Solid Propellants," *Defence Science Journal,* vol. 48, no. 2, p. 197, 1998.
[8] V. S. Bozic, D. D. Blagojevi, and B. A. Anicin, "Measurement system for determining solid rocket propellant burning rate using reflection microwave interferometry," *Journal of propulsion and power,* vol. 13, no. 4, pp. 457-462, 1997.
[9] L. H. Caveny, A. J. Saber, and M. Summerfield, "Propellant Burning Rate Uniformity Identified by Ultrasonic Acoustic Emissions," *Journal of Spacecraft and Rockets,* vol. 14, no. 7, pp. 434-437, 1977.
[10] G. P. Sutton and O. Biblarz, *Rocket propulsion elements*. John Wiley & Sons, 2011.
[11] J. Hunley, "The history of solid-propellant rocketry: What we do and do not know," in *35th AIAA, ASME, SAE, ASEE Joint Propulsion Conference and Exhibit, Los Angeles, Calif., June*, 1999, pp. 20-23.
[12] M. J. Turner, *Rocket and spacecraft propulsion: principles, practice and new developments*. Springer Science & Business Media, 2008.
[13] J. Terzic, B. Zecevic, S. Serdarevic-Kadic, and A. Catovic, "Numerical simulation of internal ballistics parameters of solid propellant rocket motors," in *15th Seminar New Trends in Research of Energtic Material, Pardubice, Czech Repuvlic*, 2012, pp. 881-892.
[14] K. O. Reddy and K. Pandey, "Burnback analysis of 3-D star grain solid propellant," *International Journal of Advanced Trends in Computer Science and Engineering,* vol. 2, no. 1, pp. 215-223, 2013.
[15] H. Adel, M. Y. Ahmed, M. S. Khalil, and H. M. Belal, "Parametric Studies of Solid Propellant Axisymmetric Grains for Space Motors," presented at the AIAA SCITECH 2023 Forum, 2023.
[16] E. M. Landsbaum, "Erosive burning of solid rocket propellants-a revisit," *Journal of Propulsion and Power,* vol. 21, no. 3, pp. 470-477, 2005.